doi:10.1016/j.jmb.2012.02.012 J. Mol. Biol. (2012) 418, 103–116

Contents lists available at www.sciencedirect.com

Journal of Molecular Biology

journal homepage: http://ees.elsevier.com.jmb

Structural Basis for Profilin-Mediated Actin Nucleotide Exchange

Jason C. Porta[1] and Gloria E. O. Borgstahl[1,2*]

[1]*Department of Biochemistry and Molecular Biology, 987696 Nebraska Medical Center, Omaha, NE 68198-7696, USA*
[2]*The Eppley Institute for Research in Cancer and Allied Diseases, 987696 Nebraska Medical Center, Omaha, NE 68198-7696, USA*

Received 24 October 2011; received in revised form 1 February 2012; accepted 6 February 2012
Available online 22 February 2012

Edited by G. Schulz

Keywords:
protein–protein interaction;
ATP;
calcium;
conformational change;
domain motion

Actin is a ubiquitous eukaryotic protein that is responsible for cellular scaffolding, motility, and division. The ability of actin to form a helical filament is the driving force behind these cellular activities. Formation of a filament depends on the successful exchange of actin's ADP for ATP. Mammalian profilin is a small actin binding protein that catalyzes the exchange of nucleotide and facilitates the addition of an actin monomer to a growing filament. Here, crystal structures of profilin–actin have been determined to show an actively exchanging ATP. Structural analysis shows how the binding of profilin to the barbed end of actin causes a rotation of the small domain relative to the large domain. This conformational change is propagated to the ATP site and causes a shift in nucleotide loops, which in turn causes a repositioning of Ca^{2+} to its canonical position as the cleft closes around ATP. Reversal of the solvent exposure of Trp356 is also involved in cleft closure. In addition, secondary calcium binding sites were identified.

Introduction

Actin is a biologically important molecule that is highly conserved and has many different functions.[1] The dynamic nature of actin is central to all forms of cellular motility, including actin-based motility of bacteria[2] and eukaryotic cells, where actin filament growth at the leading edge drives cellular motion.[3] Due to the high demand for actin to participate in a large number of processes, it is no surprise that actin has been shown to adopt many structures.[4,5] Actin has two main forms: a monomeric globular G-actin bound to an actin binding protein and a filamentous F-actin composed of an actin polymer. There are hundreds of actin binding proteins that regulate the polymerization, organization, and function of actin filaments.[6] F-actin hydrolyzes adenosine-5′ triphosphate (ATP) to ADP with the aid of a bound metal (e.g., Mg^{2+}).[7] This event occurs shortly after G-actin is added to the barbed end of F-actin. Actin-based motility is achieved by a treadmilling mechanism where F-actin moves by growing at one end (barbed end) while disassociating at the other end (pointed end). Actin monomers that have been released from the pointed end can eventually be reused, provided that the ADP is exchanged for ATP.

In mammals, profilin facilitates this nucleotide exchange and then helps deliver actin to the barbed end of a new filament,[8,9] although this function of profilin is not completely evolutionarily conserved.[10–12] In mammals, profilin binds to actin and accelerates the exchange of ADP for ATP.[8] Profilin binds to the barbed end of actin and enhances barbed-end elongation.[13] It is also thought that the free energy of ATP hydrolysis for filament

*Corresponding author. The Eppley Institute for Research in Cancer and Allied Diseases, 987696 Nebraska Medical Center, Omaha, NE 68198-7696, USA. E-mail address: gborgstahl@unmc.edu.

Abbreviations used: PDB, Protein Data Bank; SAS, solvent-accessible surface.

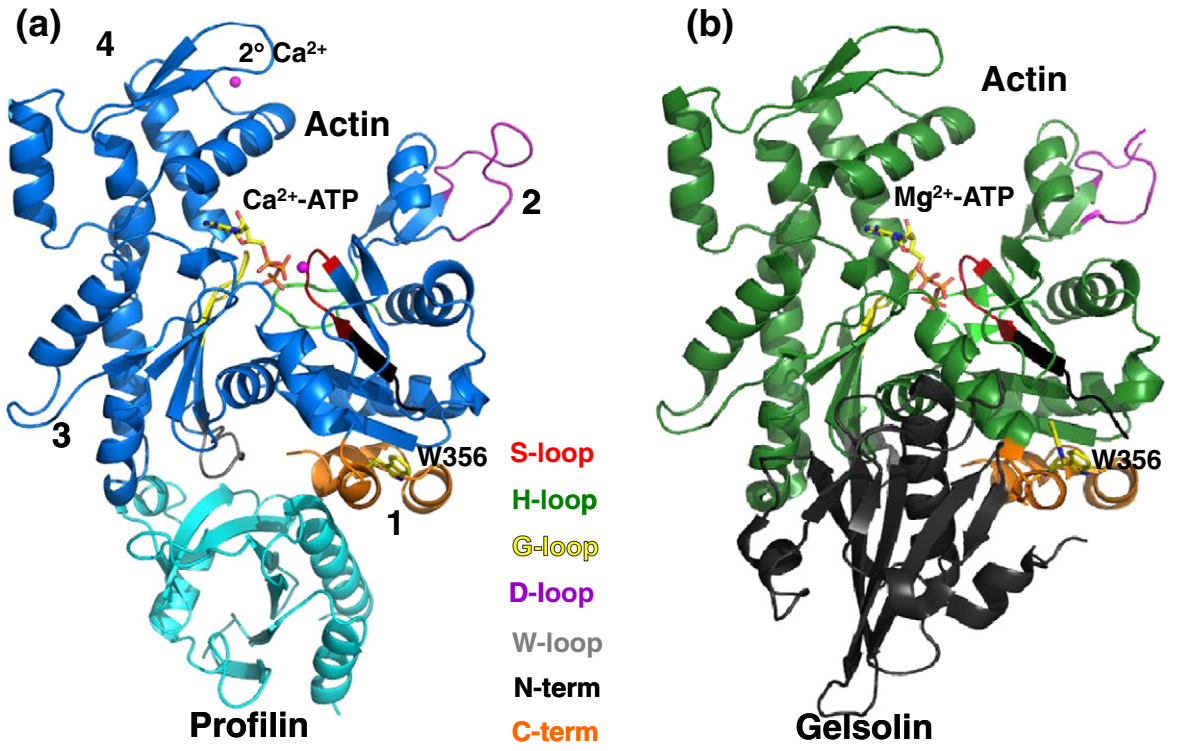

Fig. 1. Actin structure. (a) Wide-open state of bovine profilin–β-actin (PDB ID: 3UB5). (b) Nonexchanging closed state of gelsolin–pY53 actin. Subdomains 3 and 4 make up the large domain, whereas subdomains 1 and 2 make up the small domain. ATP is shown as sticks bound to Ca^{2+} (magenta sphere). Profilin (cyan) is bound to actin at subdomains 1 and 3. Gelsolin (gray) is bound to actin (green) at subdomains 1 and 3. Actin loops are colored as follows: S-loop (residues 11–16), red; H-loop (residues 70–78), green; G-loop (residues 154–161), yellow; D-loop (residues 38–52), purple; W-loop (residues 165–172), gray; N-terminus (residues 1–10), black; C-terminus (residues 349–375), orange.

growth is used by profilin, although this topic is still debatable.[14] Formin dimers nucleate unbranched actin filaments and require profilin.[15] Nucleation is achieved by binding actin to the FH2 domain of formin; this stabilizes an actin dimer.[16] The FH1 domain of formin contains a proline-rich region that binds profilin. Profilin binding to FH1 has been shown to stimulate elongation by increasing the concentration of profilin-bound G-actin at the filament barbed end.[17] Once actin binds to formin, a stable nucleus is formed; formin remains bound to the barbed end and acts as a processive elongation factor.[18] Profilin affinity for actin is also greatly lowered by the binding of phosphatidylinositol-4,5-bisphosphate at the inner leaflet of the plasma membrane.[11] Evidence suggests that this process of phosphatidylinositol-4,5-bisphosphate-mediated actin release is coordinated by a series of cell signals, which leads to actin incorporation into a growing filament.[19,20] Clearly, the profilin–actin complex is important in actin filament formation.

The first crystal structures of profilin–actin showed that profilin binds to the W-loop and C-terminal loop at the barbed end of actin (Fig. 1a). The profilin–actin structures had two forms: one that was wide open to solvent and another with a closed nucleotide cleft.[4,21,22] The domain motions between these two structures have been described as two rigid cores whose relative motion occurs at two shear regions.[23] Several exterior loops were also found to move in a hinge-like fashion (see Fig. 4 in Page *et al.*[23]). Also, a profilin–actin structure with a $VASP_{202–244}$ fragment bound to profilin with a partially open nucleotide binding cleft was solved.[24] This provides an excellent intermediary for studying actin cleft closure, and a rotation of 4.7° was observed between the two major actin domains.[24] Also, a computer simulation showed that wide-open actin closes when profilin disassociates.[25] The closure of the active site around ATP completes nucleotide exchange.

Gelsolin is an actin binding protein that has filament-severing and capping functions, which lead to the disintegration of F-actin (Fig. 1b).[26] Gelsolin first binds to the side of F-actin and causes a kink. Once a kink is made, gelsolin severs F-actin and remains bound to cap the barbed end. The capping of the barbed end ensures that this smaller and newly formed filament cannot further polymerize. In effect, the severing of F-actin into smaller

fragments by gelsolin decreases the viscosity of the cytoplasm, creating the "gel"-to-"sol" transformation that gave gelsolin its name.[27]

Gelsolin and profilin have opposite effects on actin nucleotide exchange. By measuring the fluorescent signal as ethano-ATP replaced bound ATP, Baek *et al.* showed that a complex of actin and gelsolin segment G1 inhibited nucleotide exchange.[24] They also showed that the profilin–actin complex increased nucleotide exchange. If the actin in either complex is phosphorylated at Tyr53, the initial rate of nucleotide exchange decreases, and the gelsolin complex does not exchange. Thus, the structure of pY53 actin and gelsolin represents a "nonexchanging closed" form of actin (Fig. 1b), and profilin–actin structures represent open conformations that can exchange nucleotide (Fig. 1b). A conformational change in actin's D-loop was also implicated in nucleotide exchange.[28] Although there has been a great deal of research on the topic, the complete structural basis for the nucleotide exchange mechanism has not been described. Here we describe the changes induced in the bound ATP as profilin exchanges actin's nucleotide and how these structural changes propagate from the W-loop and C-terminal loop at the barbed end to close the S-loop, H-loop, and D-loop in the nucleotide binding site and cleft.

Results and Discussion

Structure

In this study, the wide-open and closed profilin–actin crystal structures originally described by Schutt *et al.*[21] and Chik *et al.*[22] were completely redetermined using cryocooling techniques in order to obtain higher-resolution structures. The best reagents for cryocooling the closed and wide-open profilin–actin crystals were 7 M sodium formate and 35% glycerol, respectively. Also, to prevent the spontaneous formation of higher-order actin structures in the crystal, we removed excess Ca^{2+} from the bathing solution. Overall, these actin crystal structures show a similarity with other reported structures.[4,22,24] Actin is composed of two major domains: a small domain, further divided into subdomains 1 and 2, and a large domain, consisting of subdomains 3 and 4 (Fig. 1a).[29] A fold consisting of a central five-stranded β-sheet and three α-helices defines the general actin structure.[30] Wide-open profilin–actin was refined to 2.2 Å resolution with a final R_{cryst}/R_{free} of 21.4%/29.1%. The actin of the refined wide-open-state profilin–actin coordinates superposes with the starting structure [Protein Data Bank (PDB) ID: 1HLU] with an r.m.s.d. of 1.3 Å. Ramachandran analysis in MolProbity[31] indicates that 93.1% of the residues lie in the most favored region, with 1.6% existing as outliers. Closed-state profilin–actin was refined to 2.6 Å resolution with a final R_{cryst}/R_{free} of 25.1%/32.7%. Superposition of actin molecules between our closed state and the starting structure (PDB ID: 2BTF) overlays with an r.m.s.d. of 0.8 Å. Ramachandran analysis in MolProbity indicates that 90.4% of the residues lie within the most favored regions, with 1.8% existing as outliers. Overall, the structures refined well, with reasonable stereochemistry (Table 1).

Table 1. Data processing and refinement statistics

	Wide open	Closed
Data		
PDB ID	3UB5	3U4L
Space group	$P2_12_12_1$	$P2_12_12_1$
Unit cell dimensions *a*, *b*, *c* (Å)	38, 72, 186.8	38.3, 71.1, 172.0
Resolution range (Å)	85–2.2	85–2.6
Number of unique reflections	26,998	14,947
Average redundancy	3.2	5.8
Completeness (%)[a]	95.4 (71.8)	98.3 (97.4)
I/σ[a]	6.8 (2.2)	5.4 (2.0)
R_{sym} (%)[a,b]	5.9 (23.3)	9.1 (37)
Refinement		
Number of atoms		
Protein	3914	3789
ATP	31	31
Calcium	2	2
Solvent	143	27
R_{cryst} (%)	21.4	25.1
R_{free} (%)	29.1	32.7
Estimated coordinate error (Å)	0.35	0.54
Geometry		
r.m.s.d. bonds (Å)	0.014	0.012
r.m.s.d. angles (°)	1.86	1.67
Average *B*-factors (Å^2)		
Protein	36.2	44.5
Calcium	51.7	34.8
ATP	40.8	51
Water	34.3	33.2
Ramachandran analysis		
Bad rotamers (%)	6.4	6.7
Ramachandran, outliers (%)	1.4	1.8
Ramachandran, favored (%)	92.9	90.4

[a] All values in parentheses are for the highest-resolution shell.
[b] $R_{sym} = \sum_{hkl} w_i(|I_i - I_{mean}|) / \sum(I_i)$.

In order to determine the structure of the D-loop, we omitted residues 41–49 from the map calculation. Following refinement, omit $F_o - F_c$ electron density was still weak, so omit maps were recalculated at 3 and 4 Å. At lower resolution, a more clearly interpretable electron density was seen, each residue was manually fitted and refined, and the resolution was extended to 2.2 Å. The D-loop was partially ordered in the wide-open profilin–actin (Fig. 2a). When compared to the nonexchanging-closed-state structure (PDB ID: 3CI5), of which a partial D-loop was determined, a superposition of the large domains shows an overall similar secondary structure for the D-loop (Fig. 2b).

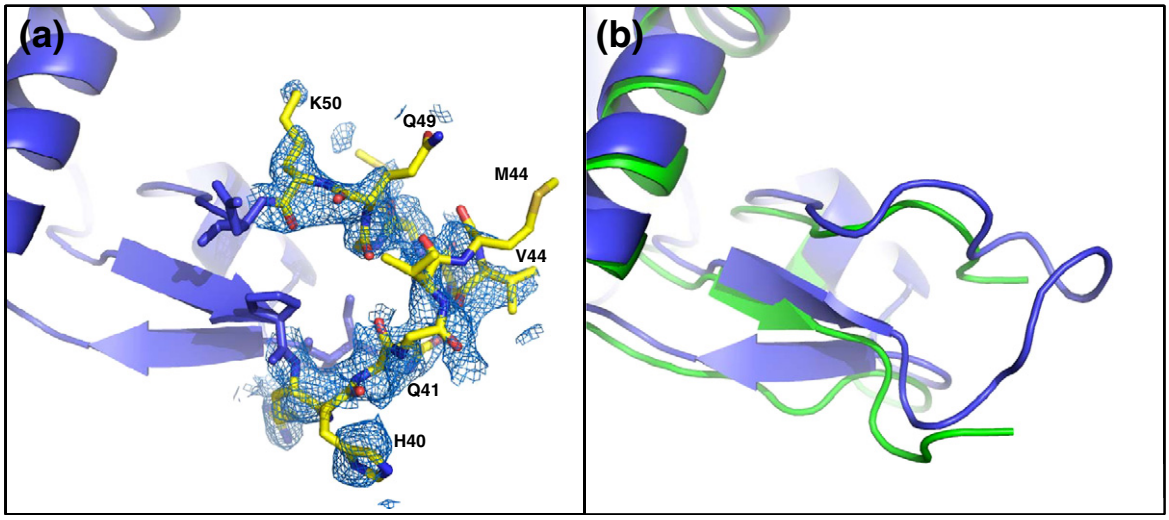

Fig. 2. D-loop conformation. (a) $2F_o - F_c$ electron density (0.8σ) of the D-loop of the wide-open-state profilin–actin covering residues 41–49. (b) Overlay of the wide-open-state profilin–actin (blue) with the partially modeled D-loop of nonexchanging closed actin (green). The modeled loops are shifted but show a similar overall structure.

Comparison of these structures with those determined by Baek *et al.* allowed for the construction of a continuum of states, which actively show the conformational changes required for actin cleft closure involved in nucleotide exchange.[24] In this report, we examine the major differences in actin structure and function between the wide open, partially open, and nonexchanging closed states. Comparison of these structures has allowed us to analyze the major conformational changes that occur when actin is opened by profilin and binds ATP and when the nucleotide binding cleft is closed by gelsolin binding. Specifically, the contributions of the individual actin loops (W-loop, S-loop, D-loop, H-loop, G-loop, and C-terminal loop) were analyzed. The closure of the actin cleft involves a rotation of the large actin domain, relative to the small domain, as ATP lands into the binding pocket. Also, we discuss the implications of profilin binding to the actin-nucleotide-sensing W-loop and how the conformational changes induced by profilin propagate to the nucleotide binding loops and cleft.

Nucleotide binding

In both the wide-open state and the closed state, there was clear interpretable density for modeling ATP binding (Fig. 3a and c). The hydrogen bonding between ATP and surrounding residues is less extensive for the wide-open structure (Fig. 3b and d). The position and orientation of the wide-open-state ATP were modeled differently from the original search model (PDB ID: 1HLU) and are now in agreement with other actin structures. One major feature is the upward kinking of α-phosphate in the wide-open state. In fact, this phosphate position appears to have more than one position, as indicated by a lack of electron density for α-phosphate compared to β-phosphate and γ-phosphate (Fig. 3a). Therefore, ATP seems to be flexible and partially exchanging. The position of Ca^{2+} is also different from that in the 1HLU structure and is positioned on the other side of the β-phosphate, where it makes hydrogen bonds with the backbone residues Gly15 and Met16.

The closed-state ATP can be seen in the standard conformation along with bound Ca^{2+}. The electron density is continuous, indicating that the ATP is moving less when compared to the wide-open state. When the large domains of our closed-state actin are superposed with the nonexchanging-closed-state actin (PDB ID: 3CI5), the ATP molecules overlay in the same conformation (Fig. S1). Ca^{2+} makes two coordinating bonds with oxygens on the β-phosphate and γ-phosphate of ATP. From the $F_o - F_c$ omit density, it can be seen that there is one clear position for the nucleotide and the metal. The position of Ca^{2+} also agrees well with the nonexchanging closed state. Whereas the nucleotide in the wide-open state is slightly shifted out of the binding cavity, the closed-state nucleotide assumes the standard position.

There are interesting differences in ATP binding between the wide-open actin and the nonexchanging closed actin. A list of close contacts between ATP and actin (up to 3.5 Å) for these two structures is given in Table 2 and Fig. S2. As the nucleotide binding cleft closes, the S-loop (residues 14–16) moves towards ATP by 2.9 Å (Fig. 4) and creates hydrogen bonds with ATP (Table 2). Also, Lys18 moves in and provides charge compensation for the buried phosphates. Asp157 and Gly302 also form

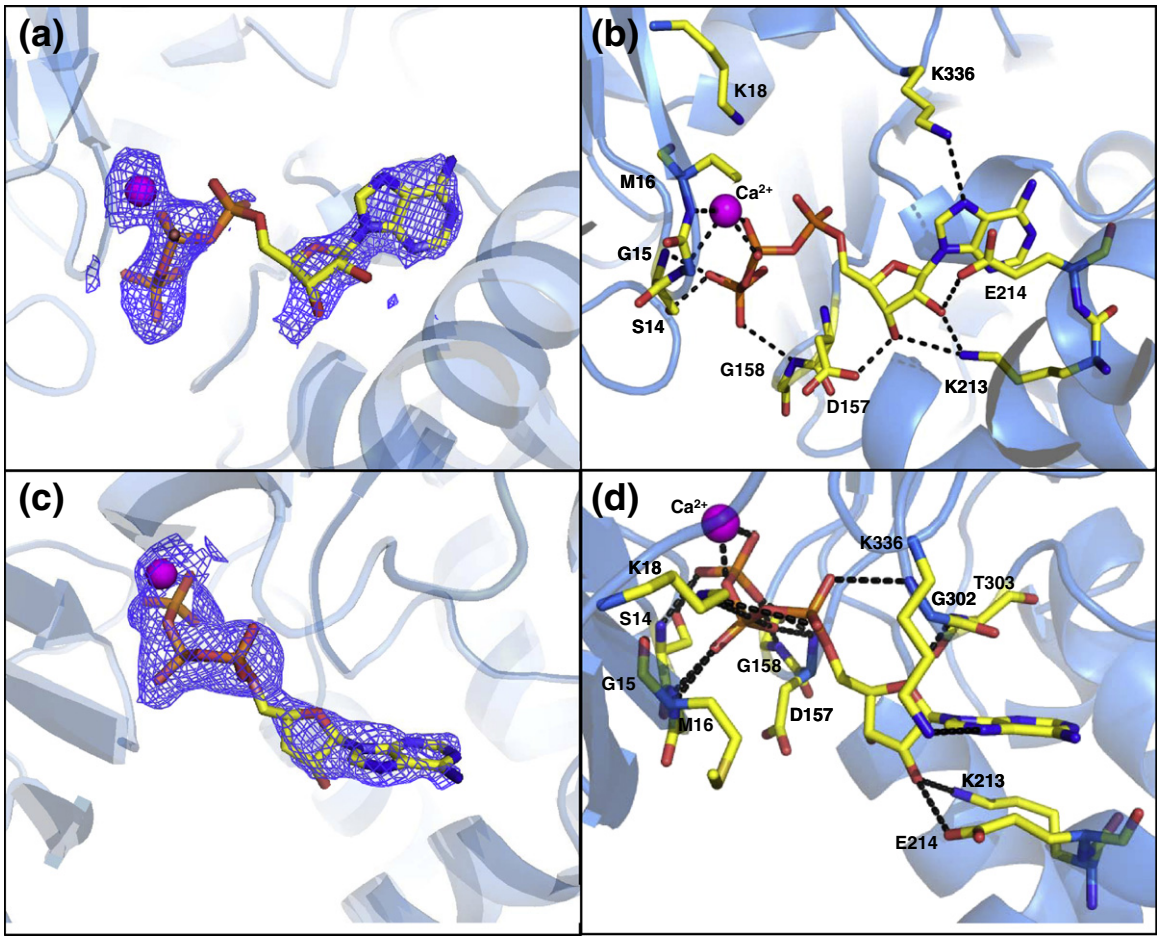

Fig. 3. Profilin–actin nucleotide binding sites. (a) Wide-open-state omit $F_o - F_c$ electron density map (2.5σ). Much of the nucleotide has ordered density, but the α-phosphate is in a bent conformation and lacks clear density. (b) Wide-open-state ATP binding site. (c) Closed-state omit $F_o - F_c$ map (2.5σ) showing continuous well-ordered density for the nucleotide and bound Ca^{2+}. (d) Closed-state ATP binding site. For (b) and (d), broken lines represent hydrogen bonds.

hydrogen bonds with ATP in the nonexchanging closed state. The conformation of ATP is similar, but the liganding metal positions are very different (Fig. 4; Fig. S2), with the closed-state metal facing the surface and coordinating four water molecules (data not shown). The interaction between Gly158 and the ATP γ-phosphate is broken; however, an additional contact is created between Asp157 and the same ATP γ-phosphate oxygen (Table 2). Note that Asp157 was modeled with two conformations in the nonexchanging closed state. With these structural changes, actin is able to close with ATP in the active site.

Concerted domain motions that close off the ATP binding cleft

The wide-open state represents the immediate binding of ATP. To visualize changes in nucleotide binding and in the protein during cleft closure, we carried out a superposition of wide-open profilin–actin, partially open profilin–actin, and nonexchanging closed actin. The actins were aligned by their large domains (residues 150–331; Fig. 4, gray). Analysis in Dyndom[33] shows a 9° rotation between the two major domains as the wide-open conformation (Fig. 4, blue) completely closes to the nonexchanging closed state (Fig. 4, green). A movie morphing these two structures is provided in Supplementary Data. When the S-loop closes, ATP and Ca^{2+} shift down and are then stably bound by actin (Fig. 3c). A concerted motion moves the D-loop 6 Å from the His40 main chain, which closes off the solvent channel, protecting ATP from the solvent. As was observed by Baek *et al.*, the partially open conformation (Fig. 4, red) transitions to the nonexchanging closed state (Fig. 4, green), which involves a smaller rotation of 5° between the large domain and the small domain.[24] Also, to see if these features were unique to the nonexchanging closed state, we

Table 2. Interactions between ATP and coordinating residues

Residue 1	Residue number	Atom	Residue 2	Atom	Distance (Å)	
					Wide-open state	Nonexchanging closed state
Lys	336	NZ	ATP	N7	3.3	3.2
Ser	14	OG	ATP	O3G	2.4	2.6
Ser	14	N	ATP	O3G	2.9	2.8
Lys	213	NZ	ATP	O3′	3.1	3.2
Lys	213	NZ	ATP	O2′	2.6	2.9
Glu	214	OE2	ATP	O2′	2.8	2.7
Asp	157	OD2	ATP	O3′	2.5	
Gly	158	N	ATP	O1G	3.1	
Asp	157	N	ATP	O1G		2.9
Met	16	N	ATP	O1B		2.8
Gly	15	N	ATP	O1B		2.9
Lys	18	NZ	ATP	O2B		2.8
Lys	18	NZ	ATP	O1A		2.8
Gly	302	N	ATP	O2A		2.8
Ca^{2+}	377	Ca	ATP	O1B	2.6	
Ca^{2+}	377	Ca	ATP	O2B	2.3	
Met	16	N	Ca^{2+}	Ca	2.4	
Gly	15	N	Ca^{2+}	Ca	3.1	
Mg^{2+}	402	Mg	ATP	O2G		1.9
Mg^{2+}	402	Mg	ATP	O2B		2.3

S-loop, residues 11–16; H-loop, residues 70–78; G-loop, residues 154–161.

performed a superposition of our closed-state actin with the nonexchanging-closed-state actin by superposing the large domains (Fig. S1). There is a striking similarity between the two structures, especially in the ATP and bound metal positions.

Based on a close-up of the active site (Fig. 4, right; Fig. S2), the overall conformations of the ATP molecules are the same. In Fig. 4a, the wide-open-state ATP can clearly be seen landing into the binding pocket and shifting into the active site of the more closed states (see Supplementary Movie). In the nucleotide binding cleft (Fig. 4b), all ATP atoms show a close agreement at the adenine ring positions. The adenine rings are practically in the same position, and the nucleotide seems to form a hinge at ribose C1′, where the wide-open-state ATP starts to rotate out of the cleft (Fig. 4a). Thus, it appears that the incoming ATP from wide-open profilin–actin aligns first at the base and sugar. This is followed by the shifting of the phosphates into the canonical position as the small domain rotates and closes (Fig. 4a). At one extreme, the phosphorus atoms of γ-phosphate are shifted by 1.8 Å. This distance decreases from the γ-phosphate back to the sugar, where the O4′ atoms are shifted by 0.6 Å. As the phosphates begin to move into the canonical position, the S-loop (containing actin residues 11–16) shifts 2.9 Å into the cavity, which in turn moves Ca^{2+} into its final closed-state position. In the top views (Fig. 4a and b, right), the wide-open-state Ca^{2+} is closer to the S-loop. In fact, rearrangements of H-bonding are pronounced here, as the oxygen atoms of the β-phosphate are now coordinated to the main chain via Ca^{2+} and not by direct H-bonding.

Motion of the well-ordered actin W-loop propagates to the active site

The actin W-loop (residues 165–172) is located at the actin barbed end and makes contacts to stabilize profilin binding. The W-loop is interesting because it lies near a hydrophobic patch (called the "hot spot"), which makes up part of an important binding site for barbed-end actin binding proteins.[12] A recent study has shown that the conformation of the W-loop is conformationally and functionally linked to the nucleotide binding pocket.[34] Also, molecular dynamics simulations predicted that the W-loop transitions from an unstructured coil to an ordered β-turn upon ATP hydrolysis.[35] However, for both the wide-open state and the nonexchanging closed state, the W-loop retains an ordered β-turn that is stabilized by backbone interactions between Tyr166 and Tyr169 (Fig. 5a). Although the conformation is the same, the W-loop is shifted 1.0 Å in the wide-open state compared to the nonexchanging closed state. This movement of the nucleotide-sensing W-loop propagates into the corresponding 1.0-Å movement of the G-loop and 2.9-Å movement of the S-loop.

Examination of the side-chain conformations and interactions explains how this movement is propagated from the W-loop to the nucleotide binding site. For the side chains of the W-loop residues, the major difference is the conformation of Glu167. In the profilin–actin interface, Glu167 stacks against profilin residue Arg88 in a strong ionic interaction. Arg88 holds Glu167 in this conformation (Fig. 5b). In the nonexchanging actin–gelsolin structure, Glu167

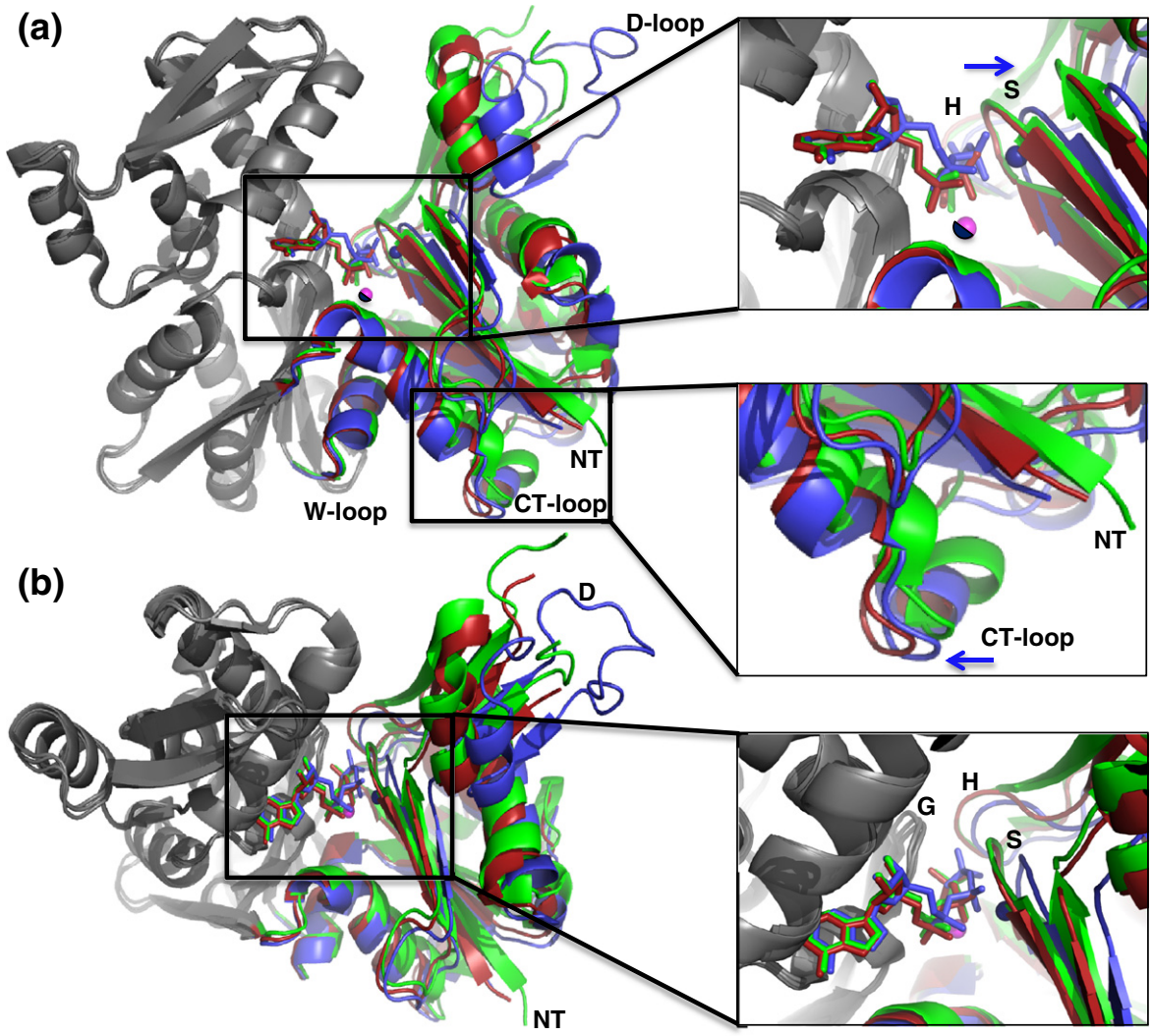

Fig. 4. The domain motions that close actin when ATP is loaded. (a) Wide-open-state actin (blue) was superimposed with partially-open-state actin (red; PDB ID: 3CHW) and nonexchanging-closed-state actin (green; PDB ID: 3CI5). Their large domains (gray; residues 150–331) were aligned using the program Superpose[32] (r.m.s.d. of 0.45 and 0.65 Å, respectively). (b) Top view of the active site and entrance to the nucleotide binding cleft. Zoomed-in views are presented on the right. Ca^{2+} and Mg^{2+} (pink) for the closed state and the partially open state have identical positions; therefore, only one atom is visible. The wide-open-state Ca^{2+} (blue) is shown in the noncanonical position.

is oriented differently, allowing for stacking with gelsolin residue Gln94 (Fig. 5c). The conformation of Glu167 when profilin is bound to actin causes a steric conflict with Thr148 of actin (Fig. 5d) that pushes the structural elements away in a rigid manner, propagating all the way to the nucleotide binding site and opening it. Profilin binds the actin barbed end in a bidentate fashion that includes interactions between actin Arg372 of the C-terminal domain and profilin Tyr128 (Fig. 5b, right side). Gelsolin binds actin differently; thus, in the nonexchanging closed state, the C-terminal domain is free to move. The net effect is the opposite motions of the C-terminal domain and the S-loop, which opens and closes the cleft (Fig. 4a, compare green and blue structures; see also Supplementary Movie). Finally, these structures show that movements in the W-loop upon actin cleft opening by profilin are linked to conformational changes in the nucleotide binding loop. These structural observations of the reciprocal communication between the W-loop and the nucleotide binding cleft are in agreement with the experimental measurements of Kudryashov *et al.*[34]

Solvent accessibility of the ATP binding site

For the ADP to be replaced with ATP, it must have a clear path to and from the surrounding solvent. A

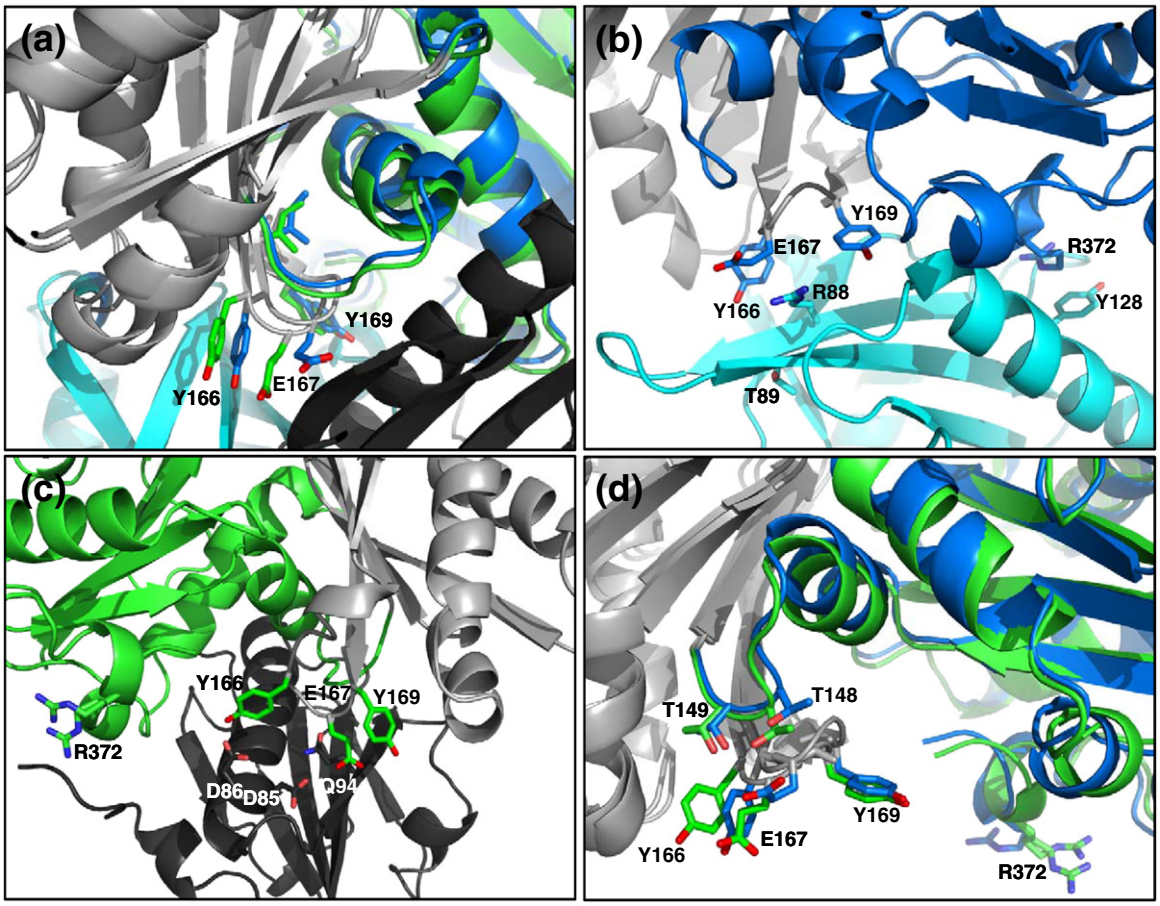

Fig. 5. Actin W-loop conformations in the wide-open and nonexchanging closed states. (a) W-loop residues for the wide-open state (blue) and the nonexchanging closed state (green) rotated +45° from standard view. Light gray denotes the superimposed regions (same as in Fig. 4); profilin and gelsolin are shown in cyan and black, respectively. (b) The W-loop of wide-open-state actin interacts with profilin to stabilize the interaction. Note the stacking interactions between actin residue Arg372 and profilin residue Tyr128. Here, actin is shown in standard view. (c) Gelsolin binds the opposite face of actin. Nonexchanging-closed-state actin W-loop residues interact with gelsolin to stabilize the interaction. Here, the structure is rotated 180° from standard view. (d) Intramolecular interactions between the actin W-loop actin residues Thr148 and Thr149. Here, actin is shown in standard view.

solvent-accessible surface (SAS) for the wide-open state shows a clear path for ATP to enter the active site or, alternatively, for ADP to be released to the solvent (Fig. 6a). From the positions of the phosphates, a large cavity opens up into a channel that leads directly to the solvent. The nucleotide base is buried and tucked into its binding pocket. When partially open profilin–actin is viewed in the same way, the channel begins to close off to the solvent (Fig. 6b). The large cavity that existed for the wide-open state has now closed off around the ATP phosphates. It can also be seen that the channel leading to the surrounding solvent is now starting to pinch off, further preventing nucleotide exchange. The SAS for nonexchanging closed actin shows that the solvent channel is completely closed so it is not possible for nucleotide to exchange (Fig. 6c). The SAS for ATP in the wide open, partially open, and nonexchanging closed states are 95.1, 56.1, and 38.5 $Å^2$, respectively.

Wide-open profilin–actin forces Trp356 to become solvent exposed

It was observed that when profilin binds to actin, there occurs a noticeable decrease in the intensity of tryptophan fluorescence, which was thought to be caused by the shielding of actin Trp356 by profilin.[24] The wide-open-state profilin–actin structure showed one clear position for Trp356 (Fig. 7a). A comparison of Trp356 side-chain orientations for the wide-open state and those for the partially-open-state structure shows differing rotamer positions (Fig. S3a). In the nonexchanging closed actin, there

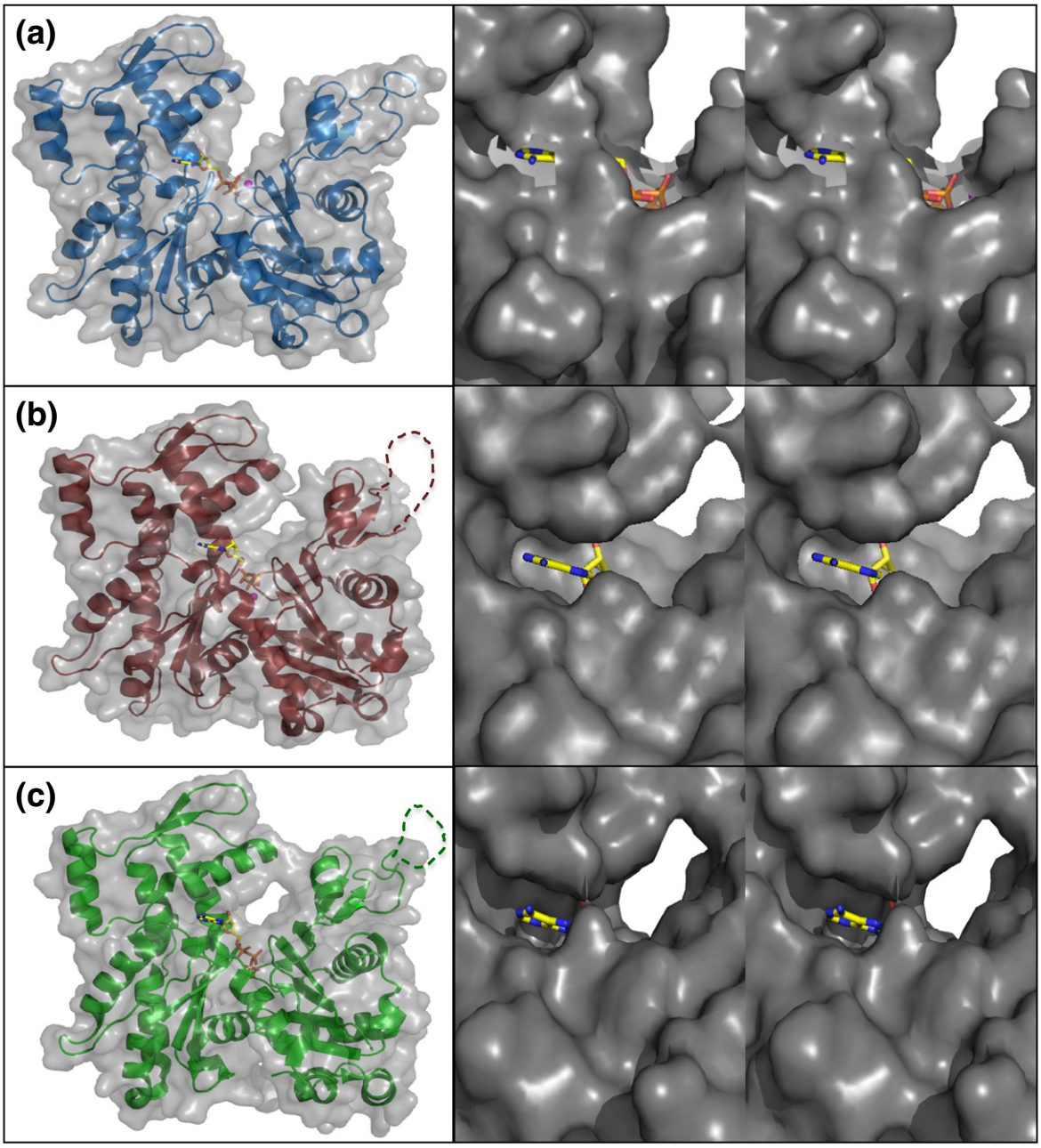

Fig. 6. The wide-open-state ATP of profilin–actin is more solvent exposed. (a) Wide-open-state profilin–actin SAS. (b) SAS of partially-open-state profilin–actin. (c) SAS of nonexchanging-closed-state actin. Zoomed-in cross-eye stereo pairs (right) show the solvent accessibility of ATP looking down the nucleotide cleft. For the zoomed-in views, the molecule was rotated 90° about the *z*-axis.

are two positions for Trp356 (Fig. 7b, green), one of which overlays the wide-open Trp356 position (Fig. 7b, blue). In our closed-state actin, there was evidence for two positions for Trp356; in the partially-open-state, Trp356 is in the buried position (Fig. S3b). In the structure of the nonexchanging profilin–actin, two conformations for Trp356 and Phe352 were determined, and it can be seen how a second and more buried conformer of Phe352 compensates for the buried Trp356 position (Fig. 7d). It can be seen in this structure how Trp356 can be buried at the actin surface due to a compensatory Phe352 dual conformer that rotates to accommodate the indole ring (Fig. 7d). Therefore, it appears that the interior position of Trp356 occurs as the small domain rotates relative to the large domain and

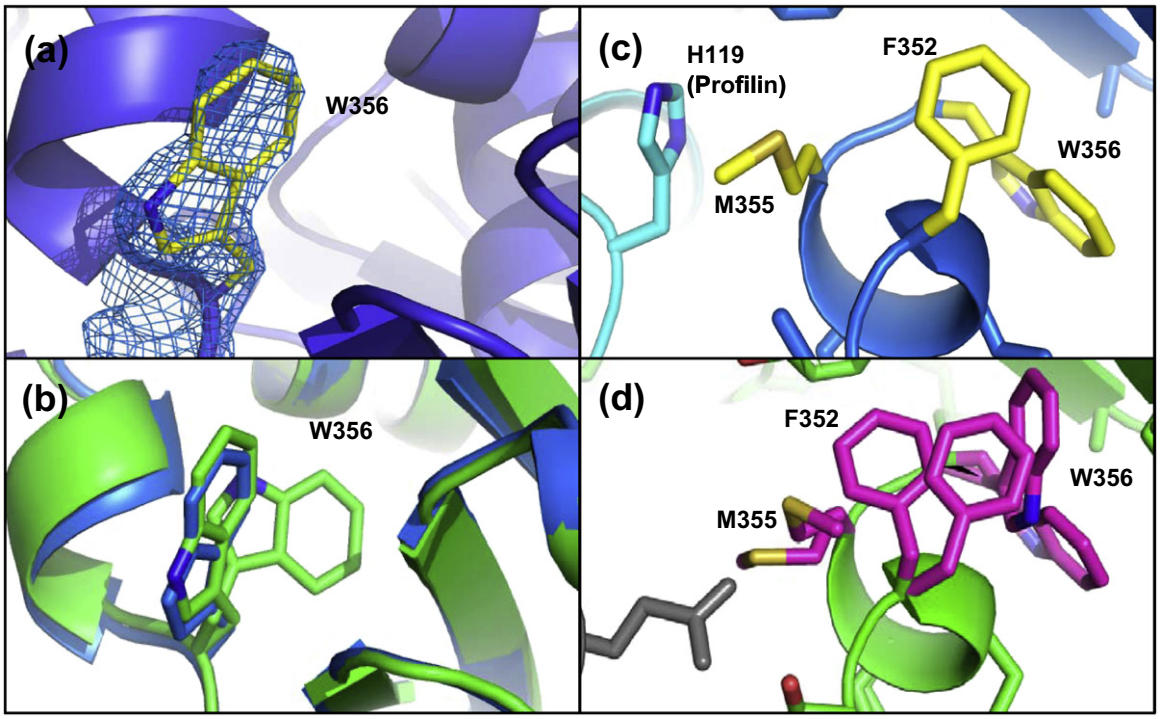

Fig. 7. Profilin prevents dual conformations for Trp356 in the wide-open state. (a) $2F_o - F_c$ density (1.5σ) for wide-open-state Trp356. (b) Trp356 single conformation in the wide-open state (blue) and dual conformations in the nonexchanging closed state (green). (c) In the wide-open state, His119 on profilin blocks the concerted motions of Met355 and Phe352; therefore, Trp356 is extended to the surface. (d) Corresponding view for the nonexchanging closed state showing the dual conformation for Met355, Phe352, and Trp365, which are not blocked by gelsolin.

actin closes upon the ATP. Clearly, the binding of profilin in the wide-open state can cause Trp356 to alter its position, as was indicated by a change in tryptophan fluorescence.[24] Structurally, this is explained by the position of His119 on profilin that contacts Met355 across the interface. There are no contacts here in the nonexchanging closed structure (Fig. 7d). The contact with profilin His119 holds Met355 in place, which consequently holds Phe352 in place and squeezes Trp356 out of the hydrophobic pocket and into the solvent (Fig. 7c). Interestingly, the unfavorable surface-exposed position of the hydrophobic Trp356 in the wide-open state probably helps make it a thermodynamically less stable state, as was observed computationally.[25]

Secondary sites of Ca^{2+} binding

It is well documented that actin contains several low-affinity binding sites for metals (i.e., Ca^{2+}, Mg^{2+}, and K^{+}).[36,37] These sites also have known regulatory roles. For example, the transformation of Ca–G-actin to a polymerizable species is mediated by the binding of Mg^{2+} to a low-affinity site, and not by replacing Ca^{2+} at the high-affinity site.[36] In this study, a couple of secondary Ca^{2+} sites for profilin–actin were found. In the wide-open state, a Ca^{2+} binding site was found coordinating with Glu205, Ser199, and Thr201 in subdomain 4 (Fig. 8a). This corresponds to a site found in uncomplexed ADP actin (PDB ID: 1J6Z).[38] For the closed-state profilin–actin, a secondary Ca^{2+} binding site was located off Asp288. Ca^{2+} makes two bonds with the Asp side chain and is coordinated by a water molecule (Fig. 8b). There was no contribution from Asp286. A similar binding of Ca^{2+} can been seen with the structure (PDB ID: 1NWK) of an uncomplexed actin in the ATP state (PDB ID: 1NWK).[39]

Conclusions

The role of the D-loop in actin nucleotide exchange has remained unclear. In an experiment that tested the proteolytic susceptibility of actin upon exchanging ATP for ADP (with Mg^{2+} as the tightly bound cation), the D-loop became more resistant to cleavage by subtilisin and a novel *Escherichia coli* protease.[28] It seems likely that this is the result of a conformational change in the D-loop, where it assumes a more compact structure. It is interesting to note that in our wide-open profilin–actin where the nucleotide is exchanging, the D-loop is much more farther away from the ATP site than in

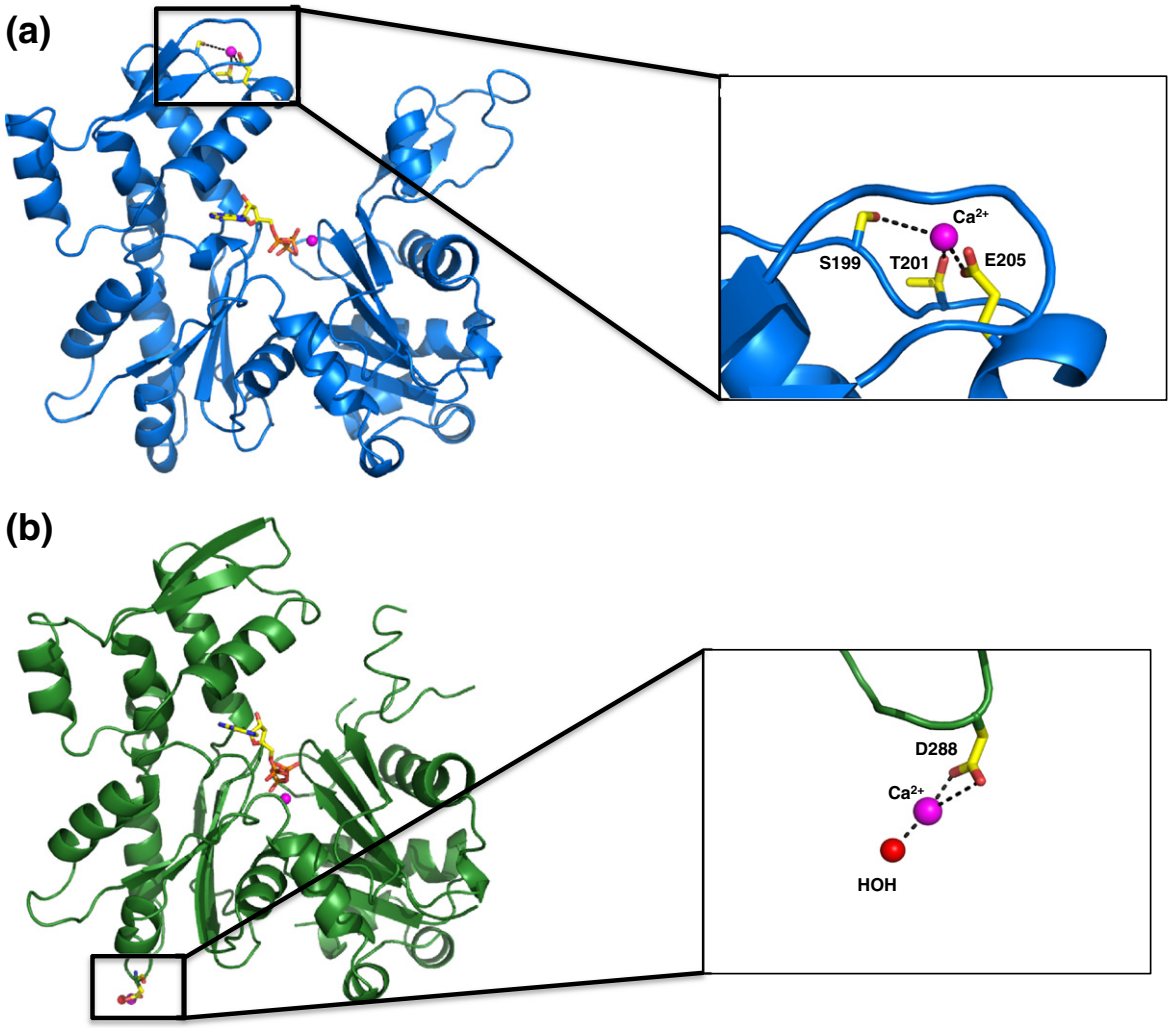

Fig. 8. Secondary Ca^{2+} binding sites on actin. (a) Secondary Ca^{2+} binding site on wide-open profilin–actin subdomain 4. (b) Secondary Ca^{2+} binding site on closed-state profilin–actin subdomain 3.

other structures. What has most frustrated our understanding of the structural basis of actin nucleotide exchange is a lack of actin structures in the open state with a modeled D-loop. Considering that the D-loop is highly mobile, this difficulty in obtaining D-loop structures likely stems from issues concerning crystal packing this flexible region into a crystal lattice. It was suggested that although the partially-open-state profilin–actin could explain the stimulation of nucleotide exchange, the short-lived state by which the nucleotide is actually released may be described by a more wide-open cleft.[24] This finding is also supported by a molecular dynamics simulation of profilin–actin, where it was shown that the wide-open state of the original room-temperature structure was a short-lived state and that the cleft immediately closed upon profilin disassociation.[25] For the ATP to enter or exit the binding pocket, the cleft would have to be wide open, and this tertiary state would likely be unstable, so it closes and becomes protected from solvent.

For the bound nucleotide to be exchanged, it must be given proper space to enter or exit the nucleotide binding cleft. Before profilin binds, the actin nucleotide binding cleft is in the closed position. Profilin then binds to actin subdomains 1 and 3, which rotate relative to each other by 4.7° to pinch around the profilin.[24] An opening of the nucleotide binding cleft subdomains 2 and 4 complements this rotation. When profilin binds the actin, the W-loop is moved by 1 Å in the wide-open state—a movement that propagates to the G-loop in the nucleotide binding pocket, causing another 1-Å shift that further stabilizes ATP binding. Therefore, it would seem that as profilin binds to the actin barbed end, the movement of the W-loop is structurally linked to the nucleotide binding site. From the SAS (Fig. 6), it was shown that a partially opened profilin–actin has a tightly packed ATP and, although the cleft is

slightly open, is still insufficient for releasing a bound nucleotide. Therefore, actin needs a mechanism by which the cleft can fully open to exchange nucleotide. The wide-open profilin–actin is shown to have a clear solvent channel leading from the nucleotide binding cleft to the bulk solvent (Fig. 6b).

Analysis of the close contacts and hydrogen bonds between the wide-open-state actin and the nonexchanging-closed-state actin shows a change in the hydrogen bonding pattern (Table 2). A 9° rotation of the small domain relative to the large domain propagates to the nucleotide binding loops, causing them to shift into the nucleotide binding cleft. The bound Ca^{2+}, which is coordinated to residues Gly15 and Met16, is pushed into the canonical position as it coordinates with the β-phosphate and the γ-phosphate. The results further show how it is the wide-open state of profilin–actin that is actively exchanging nucleotide. Since it is known that mammalian profilin rapidly increases the rate of nucleotide exchange when binding actin, it is now clearer how this mechanism occurs through the opening of the cleft and the formation of an open channel by which the nucleotide can be exchanged. On the other hand, for actin to be opened and for ADP to leave, it may follow a nearly identical yet reverse pathway.

Materials and Methods

Bovine profilin–β-actin was purified in the presence of Ca^{2+}-ATP in open form following published protocols.[40,41] Profilin–β-actin was crystallized using batch crystallization and microseeding. The purified precipitated protein was resolubilized at 10–15 mg ml^{-1} in a 5 mM phosphate (pH 7.6) buffer containing 0.5 mM ATP, 0.2 mM $CaCl_2$, and 1.0 mM dithiothreitol (DTT), and clarified by centrifugation. The resolubilized protein was then dialyzed against 1.3 M phosphate (pH 7.3) containing 0.5 mM ATP, 0.2 mM $CaCl_2$, and 1.0 mM DTT. After 8 h, a microcrystalline precipitate of actin paracrystals formed and was removed by ultracentrifugation. The supernatant was filtered with 0.22-mm Millex-GV filter units (Millipore), and 5–30 ml of hanging drops was suspended above the dialysis solution for crystallization. Microseeds were grown in unfiltered drops and used to seed the filtered hanging drops. Crystals grew to an average size of 0.5 mm × 0.35 mm × 0.15 mm in 24–36 h. Crystallization was performed in a cold room at 277 K. For the wide-open-state data, a profilin–actin crystal with dimensions of 0.5 mm × 0.3 mm × 0.1 mm was soaked in a solution of 1.8 M KPO_4 (pH 7.36) with 5 mM DTT and 1 mM ATP. The crystal was then transferred to a 10-μl drop of the same buffer, but with 35% glycerol acting as cryoprotectant. All manipulations of profilin–actin crystals took place in a cold room at 4 °C. The crystal was mounted on a MiTeGen Micromount,[42] plunged in liquid N_2, and transferred to a N_2 gas stream. Data were collected using a Rigaku FR-E superbright Cu Kα rotating-anode generator operating at 45 kV and 45 mA and fitted with a quarter-χ goniometer. Beam focusing was carried out using VariMaxHR optics for crystals with large unit cells. Diffraction images were collected on an R-AXIS IV^{++} image plate detector and processed using EVAL15.[43] For the closed-state data, a crystal was soaked in a solution of mother liquor with 7 M sodium formate acting as cryoprotectant.

The wide-open cryocooled structure was solved by molecular replacement with MOLREP software[44] and with the original room-temperature profilin–actin coordinates (PDB ID: 1HLU) as search model,[22] with Ca^{2+}, ATP, and solvent atoms removed from the initial model. The starting working *R*-value was 37% at 2.2 Å resolution and was reduced by cycles of rigid-body refinement, followed by restrained refinement using Refmac software.[45] The model was then improved by iterative cycles of crystallographic refinement and model building with Coot[46] as follows. $F_o - F_c$ maps showed a clear density for bound ATP and Ca^{2+}, as well as a site for a second Ca^{2+}. Also present was a clear density for an acetylated N-terminus for profilin. Due to a lack of interpretable electron density, actin N-terminal residues 1–5 and 41–49 of the D-loop were deleted. Low-resolution omit maps calculated at 3 and 4 Å were used to retrace the D-loop. Omit phases with minimal model bias were calculated by deleting the region of interest and neighbors within 4 Å by randomly displacing the remaining atoms 0.3-Å with Moleman2,[47] followed by restrained refinement. During the last stage of refinement, solvent waters were added. The final refinement statistics are listed in Table 1.

A cryocooled closed-state profilin–β-actin structure was solved by molecular replacement in MOLREP using PDB coordinates for room-temperature closed-state profilin-actin (PDB ID: 2BTF)[21] as search model, with ATP, Ca^{2+}, and solvent atoms removed. The starting *R*-value was 44% at 2.6 Å resolution and was reduced by rigid-body refinement, followed by restrained refinement using Refmac. $F_o - F_c$ maps showed a clear density for ATP, two calcium ions, and Cl^- that were fitted using Coot. Due to a lack of interpretable electron density, the following regions were removed from the structure: actin N-terminal residues 1–5 and subdomain 2 residues 37–50 and 65–67. The following residues were converted into Ala due to a lack of side-chain density: Y53, I64, K84, K95, R210, E224, K291, K315 of actin, and M122 of profilin. The final refinement statistics are listed in Table 1.

Accession numbers

The coordinates and structure factors for both wide-open and closed profilin-actin structures have been deposited in the PDB[34] under accession numbers 3UB5 and 3U4L, respectively.

Acknowledgements

This work was funded by the National Science Foundation (grant MCB-0718661), the Nebraska Research Initiative, and the Eppley Cancer Center (support grant P30CA036727). We would like to thank Clarence E. Schutt (Princeton University) and Uno Lindberg (Stockholm University) for useful discussions, as well as Peter Simone for technical assistance.

Supplementary Data

Supplementary data associated with this article can be found, in the online version, at doi:10.1016/j.jmb.2012.02.012

References

1. Cooper, J. A. (1991). The role of actin polymerization in cell motility. *Annu. Rev. Physiol.* **53**, 585–605.
2. Gouin, E., Gantelet, H., Egile, C., Lasa, I., Ohayon, H., Villiers, V. *et al.* (1999). A comparative study of the actin-based motilities of the pathogenic bacteria *Listeria monocytogenes*, *Shigella flexneri* and *Rickettsia conorii*. *J. Cell Sci.* **112**, 1697–1708.
3. Hoglund, A. S., Karlsson, R., Arro, E., Fredriksson, B. A. & Lindberg, U. (1980). Visualization of the peripheral weave of microfilaments in glia cells. *J. Muscle Res. Cell Motil.* **1**, 127–146.
4. Kabsch, W., Mannherz, H. G., Suck, D., Pai, E. F. & Holmes, K. C. (1990). Atomic structure of the actin: DNase I complex. *Nature*, **347**, 37–44.
5. Holmes, K. C., Popp, D., Gebhard, W. & Kabsch, W. (1990). Atomic model of the actin filament. *Nature*, **347**, 44–49.
6. dos Remedios, C. G., Chhabra, D., Kekic, M., Dedova, I. V., Tsubakihara, M., Berry, D. A. & Nosworthy, N. J. (2003). Actin binding proteins: regulation of cytoskeletal microfilaments. *Physiol. Rev.* **83**, 433–473.
7. Sheterline, P., Clayton, J. & Sparrow, J. C. (2002). Actin. *Protein Profile*, **4**, 1–2.
8. Korenbaum, E., Nordberg, P., Bjorkegren-Sjogren, C., Schutt, C. E., Lindberg, U. & Karlsson, R. (1998). The role of profilin in actin polymerization and nucleotide exchange. *Biochemistry*, **37**, 9274–9283.
9. Nyman, T., Page, R., Schutt, C. E., Karlsson, R. & Lindberg, U. (2002). A cross-linked profilin–actin heterodimer interferes with elongation at the fast-growing end of F-actin. *J. Biol. Chem.* **277**, 15828–15833.
10. Eads, J. C., Mahoney, N. M., Vorobiev, S., Bresnick, A. R., Wen, K. K., Rubenstein, P. A. *et al.* (1998). Structure determination and characterization of *Saccharomyces cerevisiae* profilin. *Biochemistry*, **37**, 11171–11181.
11. Goldschmidt-Clermont, P. J., Machesky, L. M., Baldassare, J. J. & Pollard, T. D. (1990). The actin-binding protein profilin binds to PIP2 and inhibits its hydrolysis by phospholipase C. *Science*, **247**, 1575–1578.
12. Wen, K. K., McKane, M., Stokasimov, E. & Rubenstein, P. A. (2011). Mutant profilin suppresses mutant actin-dependent mitochondrial phenotype in *Saccharomyces cerevisiae*. *J. Biol. Chem.* **286**, 41745–41757.
13. Bugyi, B. & Carlier, M. F. (2010). Control of actin filament treadmilling in cell motility. *Annu. Rev. Biophys.* **39**, 449–470.
14. Perelroizen, I., Didry, D., Christensen, H., Chua, N. H. & Carlier, M. F. (1996). Role of nucleotide exchange and hydrolysis in the function of profilin in action assembly. *J. Biol. Chem.* **271**, 12302–12309.
15. Goode, B. L. & Eck, M. J. (2007). Mechanism and function of formins in the control of actin assembly. *Annu. Rev. Biochem.* **76**, 593–627.
16. Otomo, T., Tomchick, D. R., Otomo, C., Panchal, S. C., Machius, M. & Rosen, M. K. (2005). Structural basis of actin filament nucleation and processive capping by a formin homology 2 domain. *Nature*, **433**, 488–494.
17. Firat-Karalar, E. N. & Welch, M. D. (2011). New mechanisms and functions of actin nucleation. *Curr. Opin. Cell Biol.* **23**, 4–13.
18. Paul, A. S. & Pollard, T. D. (2009). Energetic requirements for processive elongation of actin filaments by FH1FH2-formins. *J. Biol. Chem.* **284**, 12533–12540.
19. Lassing, I. & Lindberg, U. (1988). Specificity of the interaction between phosphatidylinositol 4,5-bisphosphate and the profilin:actin complex. *J. Cell. Biochem.* **37**, 255–267.
20. Lassing, I. & Lindberg, U. (1988). Evidence that the phosphatidylinositol cycle is linked to cell motility. *Exp. Cell Res.* **174**, 1–15.
21. Schutt, C. E., Myslik, J. C., Rozycki, M. D., Goonesekere, N. C. & Lindberg, U. (1993). The structure of crystalline profilin–beta-actin. *Nature*, **365**, 810–816.
22. Chik, J. K., Lindberg, U. & Schutt, C. E. (1996). The structure of an open state of beta-actin at 2.65 Å resolution. *J. Mol. Biol.* **263**, 607–623.
23. Page, R., Lindberg, U. & Schutt, C. E. (1998). Domain motions in actin. *J. Mol. Biol.* **280**, 463–474.
24. Baek, K., Liu, X., Ferron, F., Shu, S., Korn, E. D. & Dominguez, R. (2008). Modulation of actin structure and function by phosphorylation of Tyr-53 and profilin binding. *Proc. Natl Acad. Sci. USA*, **105**, 11748–11753.
25. Minehardt, T. J., Kollman, P. A., Cooke, R. & Pate, E. (2006). The open nucleotide pocket of the profilin/actin X-ray structure is unstable and closes in the absence of profilin. *Biophys. J.* **90**, 2445–2449.
26. Sun, H. Q., Yamamoto, M., Mejillano, M. & Yin, H. L. (1999). Gelsolin, a multifunctional actin regulatory protein. *J. Biol. Chem.* **274**, 33179–33182.
27. De Bruyn, P. P. H. (1947). Theories of amoeboid movement. *Q. Rev. Biol.* **22**, 1–24.
28. Strzelecka-Golaszewska, H., Moraczewska, J., Khaitlina, S. Y. & Mossakowska, M. (1993). Localization of the tightly bound divalent-cation-dependent and nucleotide-dependent conformation changes in G-actin using limited proteolytic digestion. *Eur. J. Biochem.* **211**, 731–742.
29. Kabsch, W. & Holmes, K. C. (1995). The actin fold. *FASEB J.* **9**, 167–174.
30. Hurley, J. H. (1996). The sugar kinase/heat shock protein 70/actin superfamily: implications of conserved structure for mechanism. *Annu. Rev. Biophys. Biomol. Struct.* **25**, 137–162.
31. Chen, V. B., Arendall, W. B., III, Headd, J. J., Keedy, D. A., Immormino, R. M., Kapral, G. J. *et al.* (2010). MolProbity: all-atom structure validation for macromolecular crystallography. *Acta Crystallogr., Sect. D: Biol. Crystallogr.* **66**, 12–21.
32. Krissinel, E. & Henrick, K. (2004). Secondary-Structure Matching (SSM), a new tool for fast protein structure alignment in three dimensions. *Acta Crystallogr., Sect. D: Biol. Crystallogr.* **60**, 2256–2268.
33. Poornam, G. P., Matsumoto, A., Ishida, H. & Hayward, S. (2009). A method for the analysis of domain movements in large biomolecular complexes. *Proteins*, **76**, 201–212.

34. Kudryashov, D. S., Grintsevich, E. E., Rubenstein, P. A. & Reisler, E. (2010). A nucleotide state-sensing region on actin. *J. Biol. Chem.* **285**, 25591–25601.
35. Zheng, X., Diraviyam, K. & Sept, D. (2007). Nucleotide effects on the structure and dynamics of actin. *Biophys. J.* **93**, 1277–1283.
36. Carlier, M. F., Pantaloni, D. & Korn, E. D. (1986). Fluorescence measurements of the binding of cations to high-affinity and low-affinity sites on ATP–G-actin. *J. Biol. Chem.* **261**, 10778–10784.
37. Murakami, K., Yasunaga, T., Noguchi, T. Q., Gomibuchi, Y., Ngo, K. X., Uyeda, T. Q. & Wakabayashi, T. (2010). Structural basis for actin assembly, activation of ATP hydrolysis, and delayed phosphate release. *Cell*, **143**, 275–287.
38. Otterbein, L. R., Graceffa, P. & Dominguez, R. (2001). The crystal structure of uncomplexed actin in the ADP state. *Science*, **293**, 708–711.
39. Graceffa, P. & Dominguez, R. (2003). Crystal structure of monomeric actin in the ATP state. Structural basis of nucleotide-dependent actin dynamics. *J. Biol. Chem.* **278**, 34172–34180.
40. Lovelace, J. J., Murphy, C. R., Daniels, L., Narayan, K., Schutt, C. E., Lindberg, U. *et al.* (2008). Protein crystals can be incommensurately modulated. *J. Appl. Crystallogr.* **41**, 600–605.
41. Carlsson, L. (1979). *Cell Motility: The Possible Role of Unpolymerized Actin.*Uppsala University, Uppsala, Sweden; PhD Thesis.
42. MiTeGen. (2011). MiTeGen Micromounts MiTeGen, Ithaca, NY.
43. Duisenberg, A. J. M., Kroon-Batenburg, L. M. J. & Schreurs, A. M. M. (2003). An intensity evaluation method: EVAL14. *J. Appl. Crystallogr.* **36**, 220–229.
44. Vagin, A. & Teplyakov, A. (2000). An approach to multi-copy search in molecular replacement. *Acta Crystallogr., Sect. D: Biol. Crystallogr.* **56**, 1622–1624.
45. Murshudov, G. N., Vagin, A. A. & Dodson, E. J. (1997). Refinement of macromolecular structures by the maximum-likelihood method. *Acta Crystallogr. Sect. D: Biol. Crystallogr.* **53**, 240–255.
46. Emsley, P., Lohkamp, B., Scott, W. G. & Cowtan, K. (2010). Features and development of Coot. *Acta Crystallogr., Sect. D: Biol. Crystallogr.* **66**, 486–501.
47. Kleywegt, G. J. (1997). Validation of protein models from Calpha coordinates alone. *J. Mol. Biol.* **273**, 371–376.